

3D Human Mesh Estimation from Single View RGBD

Ozhan Suat¹, Bedirhan Uguz¹, Batuhan Karagoz¹, Muhammed Can Keles¹, Emre Akbas^{1,2}

¹Department of Computer Engineering and ²METU ROMER Robotics Center
Middle East Technical University, Ankara, Turkey

{ozhan.suat, bedirhan.uguz, batuhan.karagoz, can.keles, eakbas}@metu.edu.tr

Abstract

Despite significant progress in 3D human mesh estimation from RGB images; RGBD cameras, offering additional depth data, remain underutilized. In this paper, we present a method for accurate 3D human mesh estimation from a single RGBD view, leveraging the affordability and widespread adoption of RGBD cameras for real-world applications. A fully supervised approach for this problem, requires a dataset with RGBD image and 3D mesh label pairs. However, collecting such a dataset is costly and challenging, hence, existing datasets are small, and limited in pose and shape diversity. To overcome this data scarcity, we leverage existing Motion Capture (MoCap) datasets. We first obtain complete 3D meshes from the body models found in MoCap datasets, and create partial, single-view versions of them by projection to a virtual camera. This simulates the depth data provided by an RGBD camera from a single viewpoint. Then, we train a masked autoencoder to complete the partial, single-view mesh. During inference, our method, which we name as M^3 for “Masked Mesh Modeling”, matches the depth values coming from the sensor to vertices of a template human mesh, which creates a partial, single-view mesh. We effectively recover parts of the 3D human body mesh model that are not visible, resulting in a full body mesh. M^3 achieves 16.8 mm and 22.0 mm per-vertex-error (PVE) on the SURREAL and CAPE datasets, respectively; outperforming existing methods that use full-body point clouds as input. We obtain a competitive 70.9 PVE on the BEHAVE dataset, outperforming a recently published RGB based method by 18.4 mm, highlighting the usefulness of depth data. Code will be released.

1. Introduction

Human pose and shape estimation, a fundamental task in computer vision, has many applications across a variety of domains including computer graphics, healthcare, sports, and AR/VR. Significant progress has been made in estimating a 3D human body mesh model from a single RGB

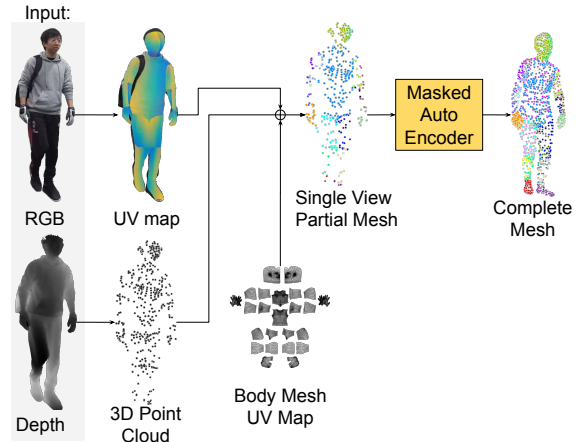


Figure 1. Inference pipeline of the proposed method, M^3 (short for “Masked Mesh Modeling”). First, we run an off-the-shelf 2D dense UV estimator on the RGB image. Then, we lift the body pixels to 3D points using depth data. Next, we match these 3D points to the vertices of a 3D human body mesh model using the UV correspondence between the pixels and the vertices of the template mesh. Finally, a masked autoencoder model completes the partial mesh to obtain the full body 3D mesh. Body Mesh UV Map image is taken from DensePose [15].

image [5, 9, 13, 20, 23, 27, 29]. These methods use a variety of training cues, including 2D [8, 21] or 3D keypoints [20], body silhouettes [41], and UV maps [14]. While these methods yield successful results in estimating human body shapes and poses, they do come with certain limitations. One notable limitation is the absence of direct depth information in RGB images, which complicates accurate 3D reconstruction, highlighting the main issue of transitioning from 2D to 3D and recovering lost data during projection. This limitation becomes especially evident when significant depth variations impact the accurate portrayal of body shapes. Additionally, the challenge extends to accurately determining the real-world scale of subjects solely from RGB images, introducing uncertainties in estimating body proportions.

There are also efforts to estimate 3D body mesh from 3D

data. Prominent methods [3, 19] typically rely on 3D scans, introducing challenges related to specialized and potentially costly equipment setups. They also involve time-intensive test-time optimization. Additionally, there had been efforts to obtain 3D human body pose from single-view RGBD data [31, 34, 40]. These pre-deep-learning and pre-SMPL [26] methods focus on finding 3D key points from single-view point clouds, and do not estimate a 3D body mesh.

In this paper, we tackle the problem of estimating a 3D human body mesh from a single-view RGBD image (Fig. 1). As RGBD cameras have become more affordable and common, this is a realistic, practical problem and a surprisingly underexplored one. Our method is highly applicable to real-world applications using a single, low-cost RGBD camera. Our multimodal method solves this problem, resulting in improved accuracy and robustness. The primary challenges in this problem are twofold:

- (i) *Accurate completion of the human mesh from partially visible RGB and depth data.* In addition to the consistent occlusion of the body surface that is not visible by the camera, body self-occlusions also contribute to the difficulty.
- (ii) *Lack of training data in the form of RGBD image and 3D mesh label pairs.* Collecting ground-truth 3D human mesh labels is both challenging and costly. Existing datasets are small and limited in environment and body pose, shape diversity.

To tackle the first challenge, inspired by the idea of Masked Image Modelling [16], we use the encoder part of a transformer-based masked autoencoder to complete a partial human mesh. To train this model, we leverage existing large-scale MoCap datasets such as AMASS [30], which contains a large and diverse set of human body shapes and poses with precise mesh models. However, they lack corresponding RGB inputs, marking the second challenge.

We address this problem by extracting a 2D UV map from the input RGB image using an off-the-shelf UV map extractor such as DensePose [15]. We obtain a point cloud of the human body with corresponding UV values by combining depth data coming from the “D” channel of the input and the 2D UV map. Next, we apply a matching algorithm to match the 3D points with the vertices of a template human mesh (e.g. SMPL [26]) to yield the partial body mesh. This partial mesh is fed to the autoencoder (described above) to finally obtain the complete human mesh.

Our training strategy for the masked autoencoder involves a two-fold process. First, we generate visible parts by projecting ground-truth body meshes (coming from a MoCap dataset) onto a fixed virtual camera, allowing us to extract visible points. Subsequently, a transformer-based model learns the relationships and patterns within the visible data, crucial for the completion process.

We employ a standard measure for evaluation, namely,

“Per Vertex Error” (PVE). Our method achieves 16.8mm and 22.0mm PVE on SURREAL and CAPE synthetic datasets, respectively. Real-world scenario testing using the BEHAVE [4] dataset resulted in 70.9mm PVE. For reference, a recently published method (TokenHMR, CVPR2024 [9]) achieves 89.3mm PVE on the same dataset, which clearly shows the benefit of using depth data. Notably, our method, which uses only a single RGBD image, also outperforms LoopReg [3] that operates on a complete (dense multiview) human body scan, on the BEHAVE dataset benchmark.

Our contributions are as follows:

- We demonstrate the potential of using single-view RGBD data for robust 3D human mesh estimation, contributing to more practical and accessible methods in various applications.
- We introduce a training method that does not require paired RGBD-mesh data, and uses a large MoCap dataset instead. In this dataset, we simulate depth measurements by placing a virtual camera around the mesh and creating 3D partial human mesh and full human mesh pairs. This allows us to train a model using simulated data and then use it with actual depth (D values) from RGBD data.
- We develop a novel model to complete a partial mesh, effectively producing a 3D human mesh model from partially visible data points, using a transformer-based encoder. Our results on synthetic and real datasets show the effectiveness of our method.

2. Related Work

Our method M^3 takes in a single-view RGBD image and produces a full body mesh. To the best of our knowledge, there is only one method (Bashirov et al. [1]) that solves the same exact task, in the literature. Although they tackle the same task as us, our training settings are completely different. They take a direct supervision approach, where they collect a dataset of 56 people using a calibrated rig of five Kinect sensors. Then, they produce “ground truth” using a “slow per-frame optimization based fitting process”. Unlike them, we train M^3 exclusively on an existing MoCap dataset without any paired RGB data. The code they provide is a demo that specifically requires an Azure Kinect. And they only report results on their own dataset. For these reasons, we could not make any comparisons. Below, we review existing work that are related to M^3 in several aspects.

Single-view RGBD input. Before the rise of deep learning (2012) and the proposal of the parametric body mesh model SMPL [26], there had been efforts to use single-view RGBD and estimate 3D human pose. These methods typically process single-view point clouds to derive 3D human body skeletons. Specifically, Shotton et al. [34] utilizes

body part labels for 3D pose estimation, while Ye et al. [40] leverages pre-computed 3D human poses to enhance 3D human pose estimation from point clouds. On the other hand, other methods such as KinectFusion [31] specialize in reconstructing humans in 3D scenes from a single-view point cloud. Unlike our work, the focus of these methods is not producing a full body mesh.

2D keypoints input. SMPLify [5] fits 3D human body mesh to given 2D keypoints. They utilize a loop to fit the body mesh step by step. We leveraged a similar network to create a baseline for our method, which fits body mesh vertices to 3D vertices generated from RGBD. MPT [24] also estimates body meshes from sparse 2D keypoints using a single-pass approach and pre-train on AMASS. However, instead of projecting 2D keypoints to a virtual camera, we utilize SMPL vertices to generate partial meshes by masking non-visible vertices from the camera’s view, making our method better suited for RGBD input.

UV map based methods. In UV map-based methods for 3D human body mesh estimation, various strategies leverage RGB images for dense correspondence. Zeng et al. [42] and DIMR [38] estimate an IUUV map and feature vector from an RGB image, transferring features to the IUUV space for human mesh estimation. Similarly, Zhang et al. [45] estimate a UV map and saliency map from an RGB image, using latent features to estimate 3D locations of human mesh vertices. Densepose2SMPL [12] estimates the UV map and then utilizes an optimization loop to fit body mesh to UV estimations. On the other hand, DaNet [43] and DenseRac [39] use the UV map as an intermediate representation and use a single pass approach to estimate human mesh from the UV map. DP3D [33] estimates the UV map and then calculates rigid transformations to pose template mesh using UV values. However, our method only utilizes UV maps to find mesh indices of depth points by leveraging the dense correspondence between the UV maps and the body mesh, which allows us to find 3D locations of visible mesh vertices.

Part-based methods. Several approaches [2, 3, 10, 22, 37] leverage human body parts to enhance the accuracy of human body mesh estimations. These methods employ feature extraction from point clouds to estimate body parts. Artec [10] utilizes SE(3) networks to estimate rigid body part rotations. PTF [37] estimates occupancies for individual body parts and fits a human mesh using a loop. Our method adopts a UV map estimation strategy to establish a mapping between 3D points and the template mesh model. It shares similarities with part-based methods as it provides supervision regarding the spatial locations of 3D points on the human body.

Complete point cloud input. Methods for estimating 3D human body meshes from point clouds commonly rely on full scans [3, 11, 19, 22, 36] or multi-view RGBD data [4]. LoopReg [3] lacks robustness to input noise and necessitates noise-free, complete human body scans during testing. In contrast, our approach operates with partial 3D vertices obtained from single-view RGBD images, enhancing accessibility.

Optimization-based methods. Some methods [2–4, 37] leverage optimization loops to get the final 3D human body mesh estimation. They require a significant amount of processing time during inference. However, we are applying a single-pass approach to estimate 3D human body mesh from single-view RGBD image. It makes our method more efficient than optimization-based methods.

Sequence input. Some approaches [18, 36] use a sequence of point clouds as input. Jang et al. [18] utilize a complete point cloud sequence for pre-training and partial point clouds for training and testing. In contrast, our method operates on a single frame RGBD, eliminating the requirement for temporal information.

3. Method

We aim to recover the vertices $V \in \mathbb{N}^{N \times 3}$ of a template mesh from RGB image $I \in \mathbb{R}^{W \times H \times 3}$ and depth map $D \in \mathbb{R}^{W \times H}$. First, a dense UV estimator Φ generates a UV map U of the image I . We combine the depth map D and the UV map U to *lift* the body pixels to a point cloud P with UV values attached. Utilizing the correspondence between their UV values, we match the 3D points and the template mesh vertices. Through this matching, we obtain a partial mesh $V^{\text{in}} \in \mathbb{R}^{N \times 3}$ where only the locations of the visible vertices are valid. We denote the visible vertices obtained this way with a mask $m \in \{0, 1\}^N$. From the partial mesh V^{in} and visibility mask m , a masked autoencoder Θ recovers the locations of vertices that are not visible and denoises the visible ones.

While the UV estimator Φ is readily available, we design a transformer-based masked autoencoder for mesh completion and train it using MoCap data.

The following sections describe the mesh model we use (Section 3.1), partial mesh generation (Section 3.2), our M^3 architecture for mesh completion (Section 3.3), and training data generation (Section 3.4).

3.1. Body Model

We utilize SMPL [26] to define our template mesh. Following previous work [23], to reduce the memory and computation requirements, we subsample SMPL template mesh to $N = 1723$ vertices. To report our results, we upsample to

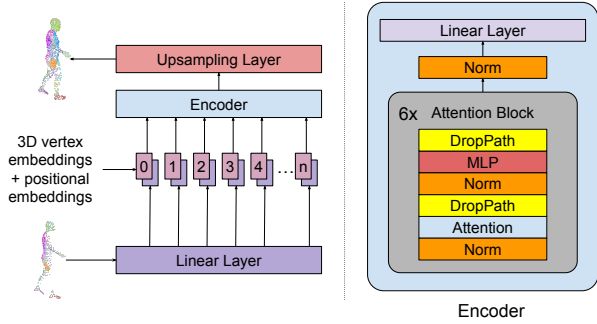


Figure 2. Architecture of our transformer-based completion model.

the original mesh using a learned upsampling layer after our MAE.

3.2. Partial Mesh Generation

The UV estimator, Φ , which generates the UV map, U , is an instance of DensePose [15] with frozen weights. We lift each pixel $p = (x, y)$ belonging to human body to 3D coordinates $\{X(p)\}$ using the intrinsics K and the depth map D :

$$X(p) = D(p)K^{-1}[x, y, 1]^T \quad (1)$$

We leverage the correspondence between the UV values predicted by DensePose and the predefined UV coordinates of SMPL vertices U_i^{vert} , where each vertex i on the SMPL model has a unique UV coordinate, to *match* the 3D points $\{X(p)\}$ with the mesh vertices. Using predefined vertex UV values U_i^{vert} , we find the point that is closest to the vertex i in terms of UV distance via nearest neighbor search:

$$V_i^{in} = X(\operatorname{argmin}_p \|U(p) - U_i^{vert}\|), \quad (2)$$

where $U(p)$ is the estimated UV coordinate of pixel p . We mask vertices with the nearest neighbor distance above a threshold to preserve the quality of partial mesh vertices, which means the UV values are considered as *matched* if they are closer than ϵ :

$$m_i = \min_p \|U(p) - U_i^{vert}\| < \epsilon \quad (3)$$

where V^{in} is mesh vertices and m is visibility mask.

3.3. Masked Mesh Modeling

Our masked autoencoder Θ (Fig. 2) embraces a Transformer-based architecture with mask tokens for non-visible vertices inspired by ViT-MAE [16]. The input to Θ consists of vertices V^{in} and their visibility mask m . The vertices V^{in} are first mapped to 3D location embeddings using a learned linear embedding layer \mathbf{E} . A learnable mask

token \mathbf{E}_{mask} is used for non-visible vertices. These 3D vertex embeddings after the addition of position embeddings \mathbf{E}^{pos} are input into the encoder:

$$z_i = \begin{cases} V_i^{in}\mathbf{E} + \mathbf{E}_i^{\text{pos}}, & \text{if } m_i = 1 \\ \mathbf{E}_{\text{mask}} + \mathbf{E}_i^{\text{pos}}, & \text{otherwise.} \end{cases} \quad (4)$$

Our encoder transforms the final embedding \mathbf{z} to the full set of 3D vertex predictions \hat{V} . An additional layer is used to upsample to the original SMPL mesh for evaluation purposes.

We train our encoder and learnable embedding layers with the overall loss term

$$\mathcal{L} = \lambda_V \mathcal{L}_V + \lambda_{3D} \mathcal{L}_{3D} \quad (5)$$

where

$$\mathcal{L}_V = \frac{1}{N} \sum_{i=1}^N \|\hat{V}_i - V_i\|_1, \quad (6)$$

$$\mathcal{L}_{3D} = \|\mathcal{J}\hat{V} - J_{3D}\|_F^2 \quad (7)$$

where V and J_{3D} are groundtruth vertices and 3D joints, respectively, and \mathcal{J} is pre-trained joint regressor matrix. Overall training pipeline of our method is given in Fig. 3.

3.4. Training Data Generation

The main advantage of our two-stage architecture is to alleviate the requirement for paired RGBD-mesh data. In principle, the UV estimator Φ and our masked autoencoder Θ can be trained separately. Since we utilize DensePose for UV estimation, the only trainable module in our pipeline is the transformer-based masked autoencoder we define in Section 3.3. To this end, we utilize human meshes fitted to MoCap data to generate input pairs of vertices V^{in} , visibility mask m . For a target mesh V , we simply add noise to it to obtain the input vertices V^{in} . The visibility mask m is calculated by ray casting from a synthetic viewpoint. Note that the 3D locations of non-visible vertices are replaced with mask tokens after embedding projection (Equation 4).

AMASS provides us with perfect data for visible surfaces; however, the same is not true on RGB images. We bridge this domain gap partially by randomly setting a percentage of visible vertices (i.e. $m_i = 1$) as non-visible. In addition, we fine-tune Θ on real data with V^{in} generated by the UV matching step outlined in Section 3.2.

4. Implementation details

We use PyTorch [32] to implement models and utilize PyKeops [7] for nearest neighbor search. We normalize input vertices to zero mean and unit variance in 3D with respect to visible ones and denormalize the encoder output. We project the normalized 3D vertex coordinates to a hidden dimension of size 20. We employ 6 transformer blocks followed by a layer normalization and a linear layer.

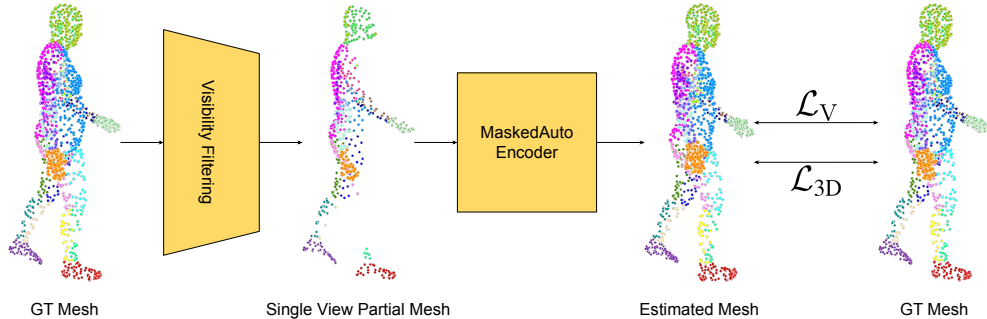


Figure 3. Training pipeline of our method, M^3 . A ground-truth body mesh, obtained from a MoCap dataset, is first downsampled and projected to a fixed virtual camera to yield the single-view partial mesh. This process simulates the “D” channel of an RGBD camera. The resulting partial mesh is then fed to the Masked Auto Encoder (MAE) which completes the mesh. The MAE is trained using vertex loss \mathcal{L}_V , and 3D loss \mathcal{L}_{3D} .

During training, we additionally mask 60% of vertices to align the real and simulated data. We also add Gaussian noise with zero mean and 0.0005 variance to the input vertices. The learning rate follows a cosine decay schedule with the first 15% of steps dedicated to warmup. The initial learning rate is $1e-3$, and weight decay is set to $1e-4$. A batch size of 32 is used during training. For fine-tuning, we disable the warmup, and the learning rate and weight decay were set to $1e-5$ and $1e-6$, respectively. A single training run takes 60 hours on a single NVIDIA A100 GPU.

5. Experiments

In this section, we present the results of our experiments, providing a thorough evaluation of our approach. To assess the accuracy and effectiveness of our method, we utilized Per Vertex Error (PVE) as the error metric. Furthermore, we conduct ablation experiments to analyze the individual contributions of different components within our methodology. We utilize two synthetic datasets, SURREAL [35] and CAPE [28], offering point cloud and ground-truth SMPL pairs. To validate our findings in real-world scenarios, we tested our method using the BEHAVE dataset, which includes paired RGBD-SMPL data.

5.1. Datasets

Training Data. We employ the AMASS dataset [30] as our training set. AMASS is a large-scale MoCap dataset with thousands of SMPL instances, providing a diverse range of motion samples as human pose and shape. It helps us to generate 3D partial mesh and SMPL pairs as described in Sec. 3.4. We use BEHAVE’s train set [4], which offers real-world RGBD-SMPL pairs, to fine-tune our model in order to adapt it to real-world scenarios.

Evaluation Data. To test our model, we utilize SURREAL [35], CAPE [28], and BEHAVE [4] datasets. SURREAL

Method	Input	PVE	
DynaBOA [†] [13]	(PAMI21)	<i>RGB</i>	70.7
PC-HMR [27]	(AAAI21)	<i>RGB</i>	59.8
Ma et al. [29]	(CVPR23)	<i>RGB</i>	44.7
Jang et al. [18]	(ICCV23)	<i>D</i> *	13.2
3DCODED [11]	(ECCV18)	<i>D</i>	41.8
Wang et al. [36]	(CVPR20)	<i>D</i>	24.3
SyNoRiM [17]	(PAMI22)	<i>D</i>	21.9
VoteHMR [25]	(ACMMM21)	<i>D</i>	20.2
PointHPS [6]	(2023)	<i>D</i>	19.6
M^3 (Ours)		<i>RGB + D</i>	16.8

Table 1. Comparison with other methods on the SURREAL dataset. The values are measured using the PVE metric in mm. *RGB* represents single view *RGB*, *D* represents single-view Depth, *PC* represents complete human Point Cloud, and (*) denotes method that take temporal data as input. (†) denotes method training on the test split with 2D supervisions.

REAL offers RGB images, depth maps, and 3D ground-truth body meshes. We are able to generate partial mesh and 3D body mesh pairs to evaluate our model. CAPE includes clothed SMPL models, and we generate partial mesh and 3D body mesh pairs for evaluation. We use BEHAVE’s test set [4] to test our model performance on real-world scenarios. We generate partial meshes from RGBD frames and evaluate our model with these RGBD-generated partial meshes and 3D human body mesh pairs.

5.2. Quantitative Results

We train our model on the AMASS dataset in our experiments and assessed its performance on multiple datasets, including SURREAL, CAPE, and BEHAVE. SURREAL and CAPE datasets provide synthetic data, while BEHAVE comprises real-world samples. We conduct a compara-

Method	Input	PVE
IP-NET [2] (ECCV20)	PC	28.2
PTF [37] (CVPR21)	PC	23.1
IP-NET [2] (ECCV20)	D	60.2
PTF [37] (CVPR21)	D	52.3
M^3 (Ours)	$RGB + D$	22.0

Table 2. Comparison with other methods on the CAPE dataset. The values are measured using the PVE metric in mm. D represents single-view Depth, PC represents complete human Point Cloud as input.

tive analysis using several methods that use single-view depth, temporal single-view depth, and complete human point cloud as input.

In Tab. 1, we compare our method with other methods that use single-view depth as input on the SURREAL dataset in terms of PVE. Our method outperforms other single-frame methods, showcasing the effectiveness of our method and the benefits of utilizing partial meshes (formed through our UV matching using the RGB channels). Our method outperforms PointHPS [6], the closest competitor that uses monocular point cloud, by 2.8mm. However, Jang et al. [18] leverages temporal information and obtains better results on the PVE metric compared to ours. As the SURREAL dataset is synthetic, it lacks noise in depth frames, which benefits the performance of all methods. To highlight the robustness of our model, discussed in Sec. 5.2.2, we introduced noise to the inputs. Additionally, our method also outperforms RGB-based methods, as shown in the table.

We also compare our method with IP-NET [2] and PTF [37]—methods capable of handling both single-view depth and complete human point cloud as input within the CAPE dataset in terms of PVE metric, as depicted in Tab. 2. Our method significantly outperforms others in single-view depth settings and even demonstrates superior performance when they utilize complete human point clouds. Specifically, our method improves PVE by 30.3mm compared to PTF [37] in the single-view depth setting. Moreover, despite using only single-view depth, our method achieves 1.1mm improvement in PVE compared to PTF using complete human point clouds as input. In addition, both IP-NET [2] and PTF [37] utilize optimization loops to obtain final results, which significantly extends the time required for the process. In contrast, our model works in a single pass without using loops, making it much more efficient.

We evaluate our model in real-world scenarios using the BEHAVE [4] dataset. Despite employing single-view RGBD compared to others using complete human point clouds or multiview RGBD frames, our method demonstrates competitive performance as shown in Tab. 3. Our approach showcases significantly superior performance com-

pared to LoopReg [3], even when provided with a complete point cloud. Our method shows relatively lower performance than IP-Net, which utilizes a complete human point cloud. We compare our model with a naive baseline, which directly fits the partial mesh to the SMPL body model using \mathcal{L}_{v2v} loss. On the other hand, our method is single pass approach while LoopReg[3], BEHAVE [4], and IPNet [2] uses an optimization loop at test time. We compared our method with the most recent RGB-based method TokenHMR [9]. Our method outperforms TokenHMR by 18.4 mm in PVE metric. This improvement demonstrates the advantage of incorporating depth information along with RGB data. We also evaluated TokenHMR using the Mean Per Joint Position Error (MPJPE) metric, resulting in 71.2 mm, whereas our method achieved 57.9 mm. Our method improves MPJPE by 13.3 mm compared to TokenHMR.

Our model exhibits a performance decline on the BEHAVE dataset in comparison to SURREAL and CAPE. The BEHAVE dataset involves subjects with loose clothing, impacting DensePose predictions by causing predictions to extend beyond the actual body boundaries. As our model relies on DensePose predictions, its performance decreases when applied to subjects with loose fitting.

Method	Input	PVE
Baseline (Opt. w/ \mathcal{L}_{v2v})	$RGB+D$	145.9
PHOSA [44] (ECCV20)	RGB	137.3
LoopReg [3] (NIPS20)	Multiview D	91.2
TokenHMR [9] (CVPR24)	RGB	89.3
IP-NET[2] (ECCV20)	PC	66.1
BEHAVE [4] (CVPR22)	Multiview D	49.9
M^3 (Ours)	$RGB+D$	70.9

Table 3. Comparison with other methods on BEHAVE dataset. D : single-view depth, PC : complete human point cloud.

Method	PVE	MPJPE
M^3	93.1	76.2
M^3 fine-tuned	70.9	57.9

Table 4. Effect of fine-tuning on the BEHAVE dataset.

5.2.1. Ablation of Fine-tuning

Given that the BEHAVE dataset is comparatively smaller in scale compared to MoCap-generated ground-truth SMPL datasets, we chose to leverage the AMASS dataset for training our network. Our model achieves respectable performance using only the AMASS dataset. However, due to the nature of the AMASS dataset not containing any RGB data, where we generate partial point clouds by projecting meshes onto a fixed camera, we extend our approach

Std of Noise (mm)	0	10	30	50
PVE	22.0	22.3	25.0	30.2

Table 5. Effect of noise on the CAPE dataset on Per Vertex Error in millimeters.

to include the BEHAVE train set for training. This adaptation results in a significant improvement in performance on the BEHAVE test set. The impact of fine-tuning on the BEHAVE dataset is shown in Tab. 4. The fine-tuning process improved our PVE result from 93.1mm to 70.9mm and MPJPE results from 76.2mm to 57.9mm.

5.2.2. Robustness to Varied Noise Levels

Depth sensor noise is a common challenge. To evaluate the robustness of our method to noisy measurements, we introduced varying levels of noise to the inputs in the SUR-REAL dataset to simulate different real-world noise scenarios and compared our performance to VoteHMR [25] (Fig. 4 in supplementary material). Each point in a test sample was offset by random 3D noise according to a given standard deviation, similar to the approach in VoteHMR. Our method demonstrated robustness to different noise levels, showing only marginal increases in the PVE metric compared to VoteHMR. We also tested our model’s robustness on the CAPE dataset by applying various types of noise to the samples. As shown in Tab. 5, our model exhibited consistent performance across varying noise levels without significant degradation, demonstrating the robustness of the masked autoencoder.

5.3. Qualitative Results

Selected samples from our qualitative results are shown in Fig. 4, demonstrating our method’s effectiveness in real-world scenarios. The images showcased effectively demonstrate our model’s ability to estimate and complete unseen parts of the human body. The samples are taken from the BEHAVE test set. Our method successfully reconstructs the 3D human mesh when a significant portion of the body is visible. Moreover, in occlusion cases where only a small portion of a body part is visible, our model effectively completes the occluded section of the corresponding body part. As shown in Fig. 4, row 3 is an example where our model accurately captures the subject’s right arm from just a few visible points.

However, it’s important to acknowledge the limitations of our model, which we illustrate in Fig. 6. In the first row, the subject’s right foot is in motion, resulting in motion blur at the right lower leg and foot. In such cases, DensePose struggles to capture these body parts from the RGB data, preventing us from accurately reconstructing depth points for those areas. This leads to errors in the reconstruction of the subject’s right leg. Additionally, heavy occlusions at

the body’s extremities can result in errors in the corresponding parts, as seen in rows 2 and 3; both have errors on the subject’s left arm.

6. Conclusions

In this study, we address the challenging task of accurate 3D human mesh estimation from single-view RGBD data, focusing on the critical problem of completing a 3D partial human body mesh.

We propose Masked Mesh Modeling (M^3), inspired by masked image modeling, to reconstruct missing points and recover full 3D meshes.

Due to the scarcity of paired RGBD-3D human body mesh data, we utilize Motion Capture (MoCap) data to create partial mesh and 3D human body mesh pairs. Following training with MoCap data, we fine-tune our model using real-world RGBD-SMPL data to enhance its applicability to real-world scenarios.

We evaluated the performance of our model on both real-world and synthetic datasets. On synthetic datasets, our approach outperforms existing single-view and multi-view methods, yielding the most favorable results. We demonstrated the robustness of our model to noise by introducing various noise levels to synthetic inputs. Furthermore, our method exhibits competitive performance on real-world datasets, underscoring its efficacy in practical scenarios. As RGBD sensors become increasingly accessible, our approach becomes applicable to real-world problems at a reduced cost.

6.1. Future Work and Limitations

The current method uses a single-view RGBD camera and generates 3D body points with the help of depth information from the camera. Our method generates an SMPL body from a partial set of human body points. Partial points can be obtained from multiview calibrated RGB cameras by triangulating DensePose estimations from multiple views. This process will take more time than our method, but there may be an increase in accuracy since partial points will come from different viewpoints. RGBD camera detects points only from one view.

We plan to extend our method to use RGB inputs alone by estimating depth from RGB data. This will allow mesh estimation without relying on RGBD sensors, broadening the applicability of our method.

References

- [1] Renat Bashirov, Anastasia Ianina, Karim Isakov, Yevgeniy Kononenko, Valeriya Strizhkova, Victor Lempitsky, and Alexander Vakhitov. Real-time rgbd-based extended body pose estimation. pages 2807–2816, 2021. 2
- [2] Bharat Lal Bhatnagar, Cristian Sminchisescu, Christian Theobalt, and Gerard Pons-Moll. Combining implicit func-

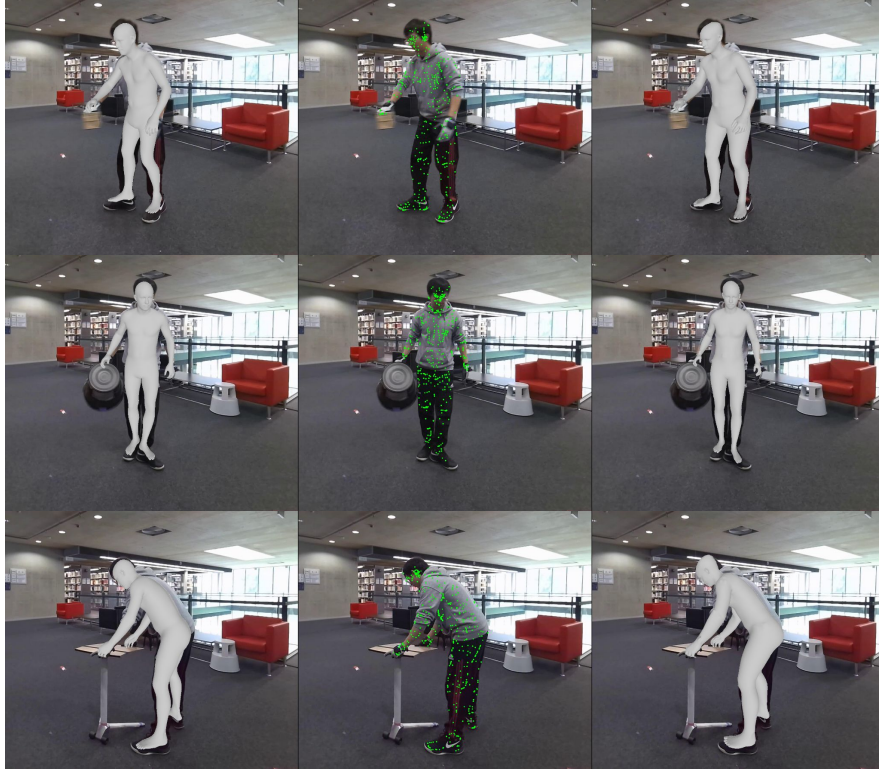


Figure 4. Visual results on BEHAVE test set. From left to right: ground truth, model inputs from RGBD, and model output.

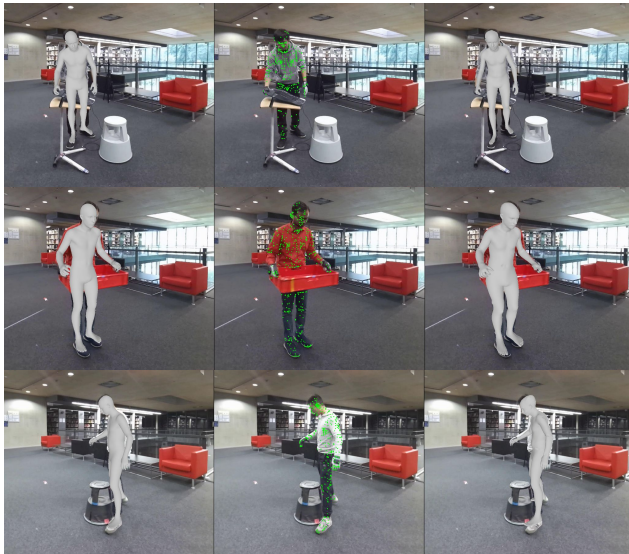


Figure 5. Occlusion examples from BEHAVE test set. The first two rows show examples where the subject is occluded by objects. The third row illustrates a case of self-occlusion: the subject's right leg is occluded by the left leg but it is correctly recovered by our model. From left to right: ground truth, model inputs from RGBD, and model output.

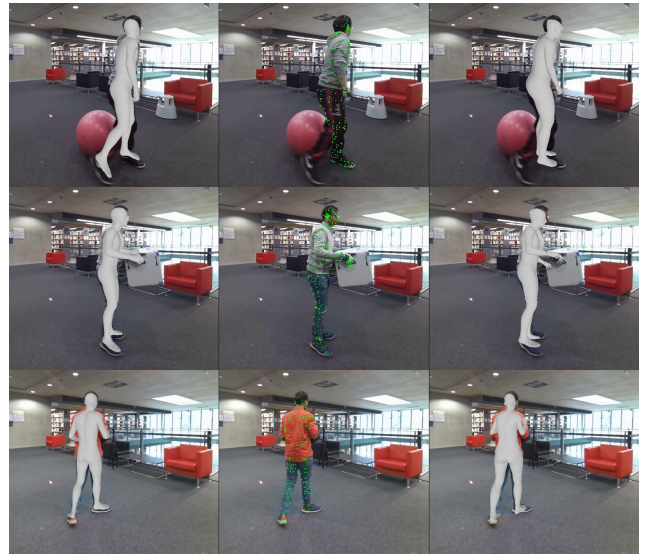


Figure 6. Failure cases on BEHAVE test set. From left to right: ground truth, model inputs from RGBD, and model output.

tion learning and parametric models for 3d human reconstruction. In *ECCV*. Springer, 2020. 3, 6

[3] Bharat Lal Bhatnagar, Cristian Sminchisescu, Christian Theobalt, and Gerard Pons-Moll. Loopreg: Self-supervised

- learning of implicit surface correspondences, pose and shape for 3d human mesh registration. *NeurIPS*, 33:12909–12922, 2020. 2, 3, 6
- [4] Bharat Lal Bhatnagar, Xianghui Xie, Ilya Petrov, Cristian Sminchisescu, Christian Theobalt, and Gerard Pons-Moll. Behave: Dataset and method for tracking human object interactions. In *CVPR*. IEEE, 2022. 2, 3, 5, 6, 1
- [5] Federica Bogo, Angjoo Kanazawa, Christoph Lassner, Peter Gehler, Javier Romero, and Michael J. Black. Keep it SMPL: Automatic estimation of 3D human pose and shape from a single image. In *ECCV*. Springer International Publishing, 2016. 1, 3
- [6] Zhongang Cai, Liang Pan, Chen Wei, Wanqi Yin, Fangzhou Hong, Mingyuan Zhang, Chen Change Loy, Lei Yang, and Ziwei Liu. Pointhps: Cascaded 3d human pose and shape estimation from point clouds. *arXiv preprint arXiv:2308.14492*, 2023. 5, 6
- [7] Benjamin Charlier, Jean Feydy, Joan Alexis Glaunès, François-David Collin, and Ghislain Durif. Kernel operations on the gpu, with autodiff, without memory overflows. *Journal of Machine Learning Research*, 22(74):1–6, 2021. 4
- [8] Hongsuk Choi, Gyeongsik Moon, and Kyoung Mu Lee. Pose2mesh: Graph convolutional network for 3d human pose and mesh recovery from a 2d human pose. In *ECCV*, pages 769–787. Springer, 2020. 1
- [9] Sai Kumar Dwivedi, Yu Sun, Priyanka Patel, Yao Feng, and Michael J. Black. TokenHMR: Advancing human mesh recovery with a tokenized pose representation. In *CVPR*, 2024. 1, 2, 6
- [10] Haiwen Feng, Peter Kulits, Shichen Liu, Michael J Black, and Victoria Fernandez Abrevaya. Generalizing neural human fitting to unseen poses with articulated se (3) equivariance. In *ICCV*, pages 7977–7988, 2023. 3
- [11] Thibault Groueix, Matthew Fisher, Vladimir G Kim, Bryan C Russell, and Mathieu Aubry. 3d-coded: 3d correspondences by deep deformation. In *ECCV*, pages 230–246, 2018. 3, 5
- [12] Dongjun Gu, Youngsik Yun, Thai Thanh Tuan, and Heejune Ahn. Dense-pose2smpl: 3d human body shape estimation from a single and multiple images and its performance study. *IEEE Access*, 10:75859–75871, 2022. 3
- [13] Shanyan Guan, Jingwei Xu, Michelle Zhang He, Yunbo Wang, Bingbing Ni, and Xiaokang Yang. Out-of-domain human mesh reconstruction via dynamic bilevel online adaptation. *IEEE TPAMI*, 45(4):5070–5086, 2022. 1, 5
- [14] Riza Alp Guler and Iasonas Kokkinos. Holopose: Holistic 3d human reconstruction in-the-wild. In *CVPR*, pages 10884–10894, 2019. 1
- [15] Riza Alp Güler, Natalia Neverova, and Iasonas Kokkinos. Densepose: Dense human pose estimation in the wild. In *CVPR*, 2018. 1, 2, 4
- [16] Kaiming He, Xinlei Chen, Saining Xie, Yanghao Li, Piotr Dollár, and Ross Girshick. Masked autoencoders are scalable vision learners. In *CVPR*, pages 16000–16009, 2022. 2, 4
- [17] Jiahui Huang, Tolga Birdal, Zan Gojcic, Leonidas J Guibas, and Shi-Min Hu. Multiway non-rigid point cloud registration via learned functional map synchronization. *IEEE TPAMI*, 45(2):2038–2053, 2022. 5
- [18] Hojun Jang, Minkwan Kim, Jinseok Bae, and Young Min Kim. Dynamic mesh recovery from partial point cloud sequence. In *ICCV*, pages 15074–15084, 2023. 3, 5, 6
- [19] Haiyong Jiang, Jianfei Cai, and Jianmin Zheng. Skeleton-aware 3d human shape reconstruction from point clouds. In *ICCV*, pages 5431–5441, 2019. 2, 3
- [20] Angjoo Kanazawa, Michael J Black, David W Jacobs, and Jitendra Malik. End-to-end recovery of human shape and pose. In *CVPR*, pages 7122–7131, 2018. 1
- [21] Nikos Kolotouros, Georgios Pavlakos, Michael J Black, and Kostas Daniilidis. Learning to reconstruct 3d human pose and shape via model-fitting in the loop. In *ICCV*, pages 2252–2261, 2019. 1
- [22] Chun-Liang Li, Tomas Simon, Jason Saragih, Barnabás Póczos, and Yaser Sheikh. Lbs autoencoder: Self-supervised fitting of articulated meshes to point clouds. In *CVPR*, pages 11967–11976, 2019. 3
- [23] Kevin Lin, Lijuan Wang, and Zicheng Liu. End-to-end human pose and mesh reconstruction with transformers. In *CVPR*, pages 1954–1963, 2021. 1, 3
- [24] Kevin Lin, Chung-Ching Lin, Lin Liang, Zicheng Liu, and Lijuan Wang. Mpt: Mesh pre-training with transformers for human pose and mesh reconstruction. pages 3415–3425, 2024. 3
- [25] Guanze Liu, Yu Rong, and Lu Sheng. VoteHMR: Occlusion-aware voting network for robust 3d human mesh recovery from partial point clouds. In *ACM MM*, pages 955–964, 2021. 5, 7, 1, 2
- [26] Matthew Loper, Naureen Mahmood, Javier Romero, Gerard Pons-Moll, and Michael J. Black. SMPL: A skinned multi-person linear model. *ACM Trans. Graphics (Proc. SIGGRAPH Asia)*, 34(6):248:1–248:16, 2015. 2, 3
- [27] Tianyu Luan, Yali Wang, Junhao Zhang, Zhe Wang, Zhipeng Zhou, and Yu Qiao. Pc-hmr: Pose calibration for 3d human mesh recovery from 2d images/videos. In *AAAI*, pages 2269–2276, 2021. 1, 5
- [28] Qianli Ma, Jinlong Yang, Anurag Ranjan, Sergi Pujades, Gerard Pons-Moll, Siyu Tang, and Michael J. Black. Learning to Dress 3D People in Generative Clothing. In *CVPR*, 2020. 5, 1
- [29] Xiaoxuan Ma, Jiajun Su, Chunyu Wang, Wentao Zhu, and Yizhou Wang. 3d human mesh estimation from virtual markers. In *CVPR*, pages 534–543, 2023. 1, 5
- [30] Naureen Mahmood, Nima Ghorbani, Nikolaus F. Troje, Gerard Pons-Moll, and Michael J. Black. AMASS: Archive of motion capture as surface shapes. In *ICCV*, pages 5441–5450, 2019. 2, 5
- [31] Richard A Newcombe, Shahram Izadi, Otmar Hilliges, David Molyneaux, David Kim, Andrew J Davison, Pushmeet Kohi, Jamie Shotton, Steve Hodges, and Andrew Fitzgibbon. Kinectfusion: Real-time dense surface mapping and tracking. In *2011 10th IEEE international symposium on mixed and augmented reality*, pages 127–136. Ieee, 2011. 2, 3
- [32] Adam Paszke, Sam Gross, Francisco Massa, Adam Lerer, James Bradbury, Gregory Chanan, Trevor Killeen, Zeming Lin, Natalia Gimelshein, Luca Antiga, et al. Pytorch: An imperative style, high-performance deep learning library. In *NeurIPS*, 2019. 4

- [33] Roman Shapovalov, David Novotny, Benjamin Graham, Patrick Labatut, and Andrea Vedaldi. Densepose 3d: Lifting canonical surface maps of articulated objects to the third dimension. In *ICCV*, pages 11729–11739, 2021. [3](#)
- [34] Jamie Shotton, Ross Girshick, Andrew Fitzgibbon, Toby Sharp, Mat Cook, Mark Finocchio, Richard Moore, Pushmeet Kohli, Antonio Criminisi, Alex Kipman, et al. Efficient human pose estimation from single depth images. *IEEE TPAMI*, 35(12):2821–2840, 2012. [2](#)
- [35] Gül Varol, Javier Romero, Xavier Martin, Naureen Mahmood, Michael J. Black, Ivan Laptev, and Cordelia Schmid. Learning from synthetic humans. In *CVPR*, 2017. [5](#), [1](#)
- [36] Kangkan Wang, Jin Xie, Guofeng Zhang, Lei Liu, and Jian Yang. Sequential 3d human pose and shape estimation from point clouds. In *CVPR*, pages 7275–7284, 2020. [3](#), [5](#)
- [37] Shaofei Wang, Andreas Geiger, and Siyu Tang. Locally aware piecewise transformation fields for 3d human mesh registration. In *CVPR*, pages 7639–7648, 2021. [3](#), [6](#)
- [38] Yanjun Wang, Qingping Sun, Wenjia Wang, Jun Ling, Zhongang Cai, Rong Xie, and Li Song. Learning dense uv completion for human mesh recovery. *arXiv preprint arXiv:2307.11074*, 2023. [3](#)
- [39] Yuanlu Xu, Song-Chun Zhu, and Tony Tung. Denserac: Joint 3d pose and shape estimation by dense render-and-compare. In *ICCV*, pages 7760–7770, 2019. [3](#)
- [40] Mao Ye, Xianwang Wang, Ruigang Yang, Liu Ren, and Marc Pollefeys. Accurate 3d pose estimation from a single depth image. In *ICCV*, pages 731–738. IEEE, 2011. [2](#), [3](#)
- [41] Zhenbo Yu, Junjie Wang, Jingwei Xu, Bingbing Ni, Chenglong Zhao, Minsi Wang, and Wenjun Zhang. Skeleton2mesh: Kinematics prior injected unsupervised human mesh recovery. In *ICCV*, pages 8619–8629, 2021. [1](#)
- [42] Wang Zeng, Wanli Ouyang, Ping Luo, Wentao Liu, and Xiaogang Wang. 3d human mesh regression with dense correspondence. In *CVPR*, pages 7054–7063, 2020. [3](#)
- [43] Hongwen Zhang, Jie Cao, Guo Lu, Wanli Ouyang, and Zhenan Sun. Learning 3d human shape and pose from dense body parts. *IEEE TPAMI*, 44(5):2610–2627, 2022. [3](#)
- [44] Jason Y. Zhang, Sam PePOSE, Hanbyul Joo, Deva Ramanan, Jitendra Malik, and Angjoo Kanazawa. Perceiving 3d human-object spatial arrangements from a single image in the wild. In *ECCV*, 2020. [6](#)
- [45] Tianshu Zhang, Buzhen Huang, and Yangang Wang. Object-occluded human shape and pose estimation from a single color image. In *CVPR*, pages 7376–7385, 2020. [3](#)

3D Human Mesh Estimation from Single View RGBD

Supplementary Material

1. Extra Qualitative Results

We have added some more qualitative results. Fig. 1 displays successful outcomes of the M^3 model. Our model can reconstruct partially visible body parts. In the first two rows, the model accurately completes the left arm of the subjects. In these examples, the upper arm orientation is estimated from lower arm information, and the model successfully completes the upper arms. The third row illustrates the successful completion of the right leg, similar to the first two rows.

Fig. 2 shows instances of minor errors. When the model lacks information about a specific body part, it may reconstruct a random orientation that aligns with visible points. In the first row, the right elbow is estimated solely based on the right hand location, and the elbow can be located in more than one place for the given input. The second row presents a similar problem. The model makes errors when estimating hand locations due to insufficient information in the input. In the third row, where the model doesn't observe any points from the right side of the body, estimations for the right body parts are inaccurate.

The model makes significant errors on some challenging examples, as in the Fig. 3. In the first case, where the middle of the body lacks any points, the model struggles to reconstruct the hip region. For body parts with only noisy sparse points, as shown in the second row, the model produces distorted shapes for those body parts. The final row shows an issue with non-visible body part reconstruction. The partial body lacks leg points, causing the model to generate shorter legs to align with dense points near the hips.

We also generated several video outputs from the BEHAVE test set. You can access the videos using the following link: tinyurl.com/maskedmeshmodelling. Each frame of the video contains 3 columns. The first column is the ground truth, the second column is the model input, and the third column is the output.

2. Robustness to Noise

We tested noise robustness by applying varying noise levels to the input, similar to VoteHMR [25]. Fig. 4 compares our method with VoteHMR. Our method demonstrates more consistent results compared to VoteHMR as the noise level increases.

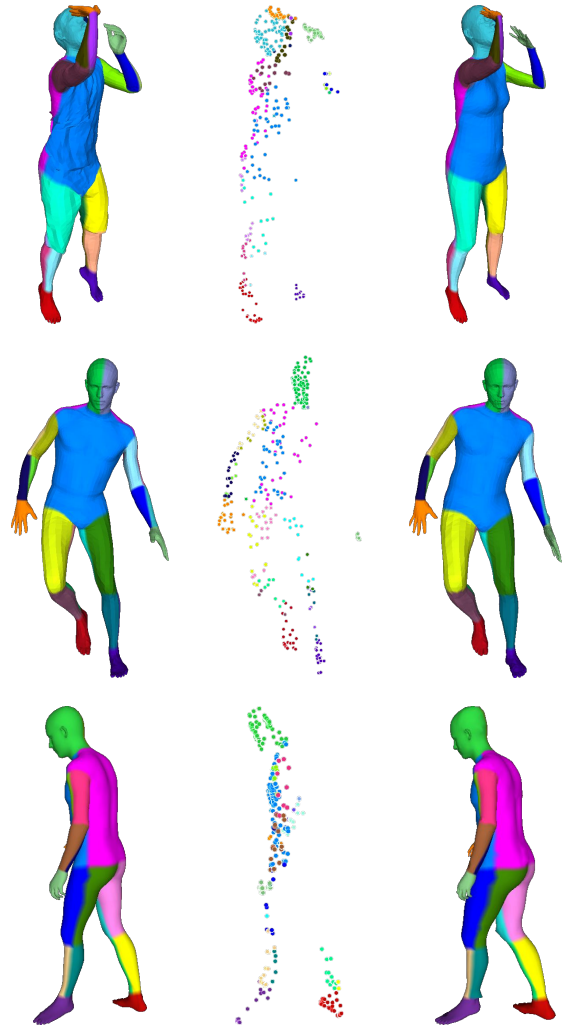


Figure 1. Estimations from CAPE [28] (First Row), SURREAL[35] (Second Row), and BEHAVE[4] (Third Row). The first column is ground truth, the second column is model input, and the third column is model output.

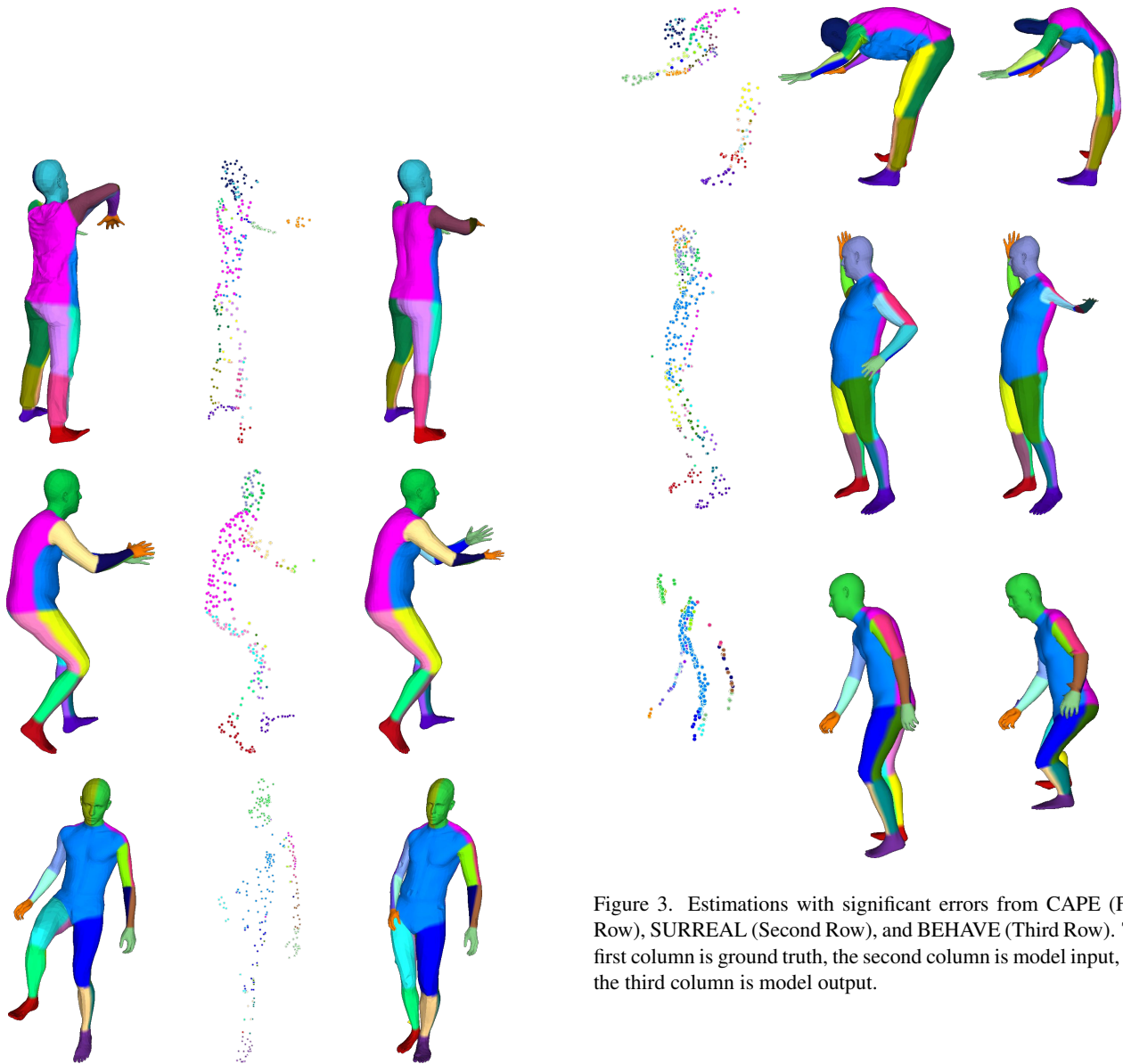


Figure 2. Estimations with minor errors from CAPE (First Row), SURREAL (Second Row), and BEHAVE (Third Row). The first column is ground truth, the second column is model input, and the third column is model output.

Figure 3. Estimations with significant errors from CAPE (First Row), SURREAL (Second Row), and BEHAVE (Third Row). The first column is ground truth, the second column is model input, and the third column is model output.

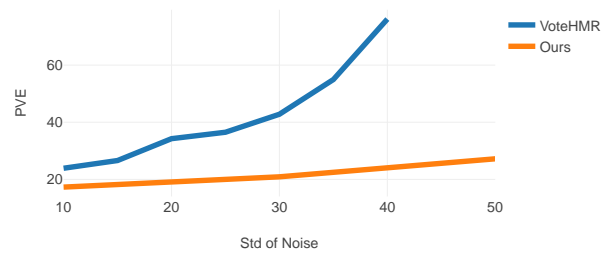


Figure 4. Comparison between our method M^3 and VoteHMR [25] regarding the effect of noise on Per Vertex Error (PVE) in mm.